Published in final edited form as:
Neuroimage. 2011 February 1; 54(3): 2096–2104. doi:10.1016/j.neuroimage.2010.10.059.

Probabilistic Analysis of Activation Volumes Generated During Deep Brain Stimulation

Christopher R. Butson[1,*], **Scott E. Cooper**[2], **Jaimie M. Henderson**[3], **Barbara Wolgamuth**[2], and **Cameron C. McIntyre**[1,2]

[1] Department of Biomedical Engineering, Cleveland Clinic Foundation, Cleveland, OH

[2] Center for Neurological Restoration, Cleveland Clinic Foundation, Cleveland, OH

[3] Department of Neurosurgery, Stanford School of Medicine, Stanford, CA

Abstract

Deep brain stimulation (DBS) is an established therapy for the treatment of Parkinson's disease (PD) and shows great promise for the treatment of several other disorders. However, while the clinical analysis of DBS has received great attention, a relative paucity of quantitative techniques exists to define the optimal surgical target and most effective stimulation protocol for a given disorder. In this study we describe a methodology that represents an evolutionary addition to the concept of a probabilistic brain atlas, which we call a probabilistic stimulation atlas (PSA). We outline steps to combine quantitative clinical outcome measures with advanced computational models of DBS to identify regions where stimulation-induced activation could provide the best therapeutic improvement on a per-symptom basis. While this methodology is relevant to any form of DBS, we present example results from subthalamic nucleus (STN) DBS for PD. We constructed patient-specific computer models of the volume of tissue activated (VTA) for 163 different stimulation parameter settings which were tested in six patients. We then assigned clinical outcome scores to each VTA and compiled all of the VTAs into a PSA to identify stimulation-induced activation targets that maximized therapeutic response with minimal side effects. The results suggest that selection of both electrode placement and clinical stimulation parameter settings could be tailored to the patient's primary symptoms using patient-specific models and PSAs.

Keywords

Neuromodulation; computational model; Parkinson's disease; subthalamic nucleus; neurostimulation

Corresponding Author (and Reprint address): Cameron C. McIntyre, Ph.D., Cleveland Clinic Foundation, Department of Biomedical Engineering, 9500 Euclid Ave. ND-20, Cleveland, OH 44195, mcintyc@ccf.org, PHONE: (216) 445-3264, FAX: (216) 444-9198.
[*]Current affiliation: Departments of Neurology & Neurosurgery, Medical College of Wisconsin, Milwaukee, WI

CONFLICT OF INTEREST

CRB, JMH, and CCM authored intellectual property related to the project methodology, and are each shareholders and paid consultants to IntElect Medical Inc.

INTRODUCTION

Over the last two decades deep brain stimulation (DBS) has evolved from an experimental technology to a well established surgical therapy for numerous disorders (Schwalb and Hamani, 2008). The clinical successes of DBS have prompted the development of continuously improving scientific techniques to quantify its effects on the nervous system, as well as provide clinical guidance on the most efficacious anatomical locations for electrode implantation and electrical parameters for stimulation. One promising direction along this line is the concept of a probabilistic brain atlas (PBA) that compiles data from multiple patients into a statistical map that can be subsequently applied to the analysis of future patients (Lemaire et al., 2007). Nowinski et al. (Nowinski et al., 2005) pioneered the application of PBAs to the study of DBS by creating probabilistic maps of therapeutic electrode locations. However, one limitation of that original work was the lack of data related to the electrical spread of stimulation. Therefore, we set out to refine the methodology to include both anatomical and biophysical factors, as well as the degree of therapeutic benefit achieved from stimulation, thereby creating a probabilistic stimulation atlas (PSA).

While the concepts underlying the PSA can be applied to any form of DBS, we elected to create an example from data acquired in Parkinson's disease (PD) patients who had DBS leads implanted in the subthalamic nucleus (STN). The effectiveness of STN DBS for PD is well established (Obeso et al., 2001; Weaver et al., 2009); however, precise definition of the optimal stimulation target within the STN region remains an issue of debate (Plaha et al., 2006; Maks et al., 2009). For example, while the STN per se was originally assumed to be the principal target of therapeutic stimulation, several groups have shown that direct stimulation of numerous anatomical components of the STN region (e.g. fields of Forel, zona incerta, etc.) can result in similar clinical outcomes. Such conclusions have been based on retrospective studies of the anatomical location of therapeutic electrode contacts (Yelnik et al., 2003; Nowinski et al., 2005; Guehl et al., 2008) as well as prospective clinical studies using alternative surgical target coordinates (Plaha et al., 2006). In turn, it is unclear if one "optimal" stimulation target exists or if there may actually be multiple target regions that differentially regulate various symptoms.

During electrical stimulation therapy it is important to recognize that the stimulation settings and electrode locations act synergistically in each patient to define the stimulation spread to surrounding neural structures (Butson et al., 2007b; Maks et al., 2009). Hence, new insights could be gained by coupling examination of the anatomical location of the active electrode contact, the electrical spread of the stimulation, and their correlation with clinical outcomes. Previously we developed methods to predict the direct neural response to DBS on a patient-specific basis which take into account the position of the electrode in the brain, the stimulation parameter settings and the impedance of the electrode contact (Butson et al., 2007b). In the present study we created multiple patient-specific models and used them to generate a probabilistic stimulation atlas (PSA) without any *a priori* assumptions about which anatomical structures were directly stimulated. To test this approach we conducted a prospective clinical evaluation of the changes in bradykinesia, rigidity, and/or paresthesias induced by 163 different stimulation settings evaluated through 28 different electrodes (7 DBS leads) in six patients. For each set of experimentally evaluated stimulation parameters we quantified the clinical response and calculated the resulting volume of tissue activated (VTA). All results were co-registered to an anatomical atlas brain to allow comparisons across the entire patient population, as well as facilitate the development of PSAs of the brain regions associated with either therapeutic effects or side effects.

METHODS

This methodological study describes the process of creating a PSA on a per-symptom basis based on quantitative clinical outcome measures and theoretical predictions of the electrical spread of DBS. The components of this approach are:

1. A patient-specific model for each member of the study cohort. The patient-specific model combines a pre-operative MRI and a post-operative MRI for electrode localization relative to pertinent anatomical structures.
2. A PSA to compile the results from all patient-specific models. The subcomponents of the PSA are: the location of each DBS lead as determined from the patient-specific models; a VTA for each distinct set of stimulation parameters at each electrode contact; a 3D lattice of voxels that contains all VTAs; and a database of clinical outcomes corresponding to each VTA.
3. An anatomical atlas to identify structures of interest. In this study we used a nonlinear warping method (Christensen et al., 1997) to register our anatomical atlas with each patient brain, and the PSA was overlaid onto the anatomical atlas to show how the results overlap with nearby structures. Alternatively, many different registration methods or anatomical atlases could be used.

We populated our PSA database with data collected from 6 DBS patients who were stimulated in the subthalamic region. The general method for creating the PSA consisted of five basic steps. First, each patient was clinically evaluated over a range of stimulation parameters and electrode contacts. Second, patient-specific computer models were constructed to determine electrode locations. Third, the electrode locations from each patient were co-registered with an anatomical atlas brain. Next, each set of experimentally tested stimulation parameters was used to predict the VTA in the context of the anatomical atlas. In the final step the PSA was compiled and overlaid on the anatomical atlas. Clinical outcome scores associated with each stimulation parameter setting were tagged to the corresponding VTA, and the scored VTAs were superimposed and averaged to identify regions that, when activated, were associated with clinical improvement. These steps are summarized in Figure 1.

Clinical Evaluation

Subjects in this study were drawn from patients with STN deep brain stimulators for treatment of Parkinson's disease at the Cleveland Clinic. At the time of surgery, all subjects had a clinical diagnosis of idiopathic (presumed Lewy body) Parkinson's disease with clear levodopa response and no dementia, as determined by a fellowship-trained movement disorders neurologist. Seven brain hemispheres were analyzed among six patients (Table 1).

At the time of testing, all subjects were at least six months post-operative and had completed the initial period of stimulator adjustments, with stable settings in the judgment of the treating clinician. All were obtaining satisfactory and expected clinical benefit from the stimulation in the opinion of the treating physician, had not developed dementia or significant neuropsychological problems, and had not undergone a change in diagnosis. Clinically defined stimulation settings were arrived at pragmatically based on clinical judgment and experience, independently of this study. All patients had bilateral Soletra implantable pulse generators (IPGs) with 3387 electrode leads (Medtronic Inc., Minneapolis, MN). Each experiment was performed in the medication off state the morning after medications were withheld from the night before. Since the off-med/off-stimulation state was uncomfortable for our subjects, we opted to leave the ipsilateral stimulator (to the side of the body being tested) turned on with the patient's clinically defined therapeutic settings, thereby improving their ability to maintain the prolonged, sustained effort and attention

which testing required. Electrode contact impedance was measured for each experimentally tested electrode at the time of the experiment and designated as high, medium or low impedance for use in the computer models (Butson et al., 2006). The Cleveland Clinic Institutional Review Board approval and informed consent were obtained before patient evaluations.

During the clinical evaluation, each of the four DBS contacts was tested during monopolar stimulation in two blocks. During the first block we determined the maximum voltage amplitude that the patient could tolerate at each contact in increments of 0.5 V. A set of tolerable stimulation parameters were selected from this range and randomized for use in the second block. The second block then consisted of quantitative measures of bradykinesia and rigidity during each randomly ordered stimulation contact and voltage combination. Each tested parameter setting consisted of a fixed pulse width (60 μsec) and frequency (130 Hz).

Bradykinesia was measured with a finger tapping exercise where the patient was instructed to tap the index finger and thumb together as quickly and accurately as possible for 15 seconds while keeping the magnitude of finger motion constant (Unified Parkinson's Disease Rating Scale (UPDRS) item 23). Finger angular velocity was measured with solid state gyroscopes (model G-1, NeuroKinetics, Edmonton, Alberta, Canada), and the bradykinesia score was determined from the peak of the resulting power spectrum. The finger tapping trials were interleaved with rigidity measurements using a clinical impedance measurement device (model RA-1, NeuroKinetics) which has been validated against UPDRS item 22 (Patrick et al., 2001). Example data for a single patient are shown in Figure 2.

Patient-Specific Computer Model

Following a previously described methodology (Butson et al., 2007b), we constructed models to identify each electrode location relative to the surrounding anatomical nuclei. First, a pre-operative T1-weighted MRI was acquired on 1.5T Siemens Magnetom Vision or Siemens Symphony scanner with a 256mm × 256mm field of view and $1mm^3$ isotropic voxels. The MRI was used to warp 3D surfaces representing the thalamus and STN to the match the patient anatomy using a non-linear, vector field based algorithm (Christensen et al., 1997). This was performed using software developed by Surgical Navigation Technologies (Medtronic Inc, Boulder, CO). The resulting deformed 3D surfaces were then used to represent the thalamus and STN in our patient-specific computer model (Figure 1, top row). It should be noted that 3D surfaces from any anatomical brain atlas or any warping technique could be used for this step, since the primary purpose of these surfaces was to provide a visual cue for anatomical relationships relative to the results of the PSA.

A second MRI was acquired post-operatively for DBS electrode localization on a 1.5T Siemens Magnetom Vision, Siemens Symphony or Siemens Allegra scanner. The acquisition sequence used in the post-operative MRI was designed to control for heating in accordance with safety studies conducted at the Cleveland Clinic (Baker et al., 2004). Analyze 7.0 (AnalyzeDirect, Lenexa, KS, USA) was used to coregister the pre- and post-operative MRI volumes using the ITK 3D registration function (Viola and Wells, 1997), followed by manual adjustment to precisely match the positions of the anterior and posterior commissures. Detailed localization of the electrode lead and four contacts was performed by isosurfacing the halo around the electrode shaft in the postoperative MRI. At successively lower isovalues, the isosurface converged onto the four electrode contacts.

Comparison of the electrode locations and VTAs across the population of patients required the use of a common anatomical space. Our approach to this problem was to determine electrode location relative to the customized 3D surfaces described above, co-register each

patient model with the anatomical atlas, and subsequently calculate all bioelectric field solutions and VTA predictions in the context of the anatomical atlas (Figure 1, middle row). The anatomical atlas consisted of a T1-weighted MRI (acquired on the same patient as the DTI data described below) and fitted 3D surfaces, as in each patient-specific model. To co-register each patient-specific model with the anatomical atlas, we used an algorithm to determine the electrode locations relative to the surrounding nuclei. The purpose of this algorithm was to place the DBS electrode as identified in the patient brain to the analogous location in the atlas brain. While this step can be done using linear registration techniques such as those employed in image analysis software like Analyze, we used an alternate method that takes advantage of the individual nuclei in each patient brain that were identified via nonlinear atlas registration. The position of each electrode was determined by measuring the distance from the centroid of each electrode contact to points on the 3D surfaces of the thalamus and STN. Both the patient-specific model and base atlas brain had the same original 3D surfaces, but with slightly different permutations to their geometry as a result of the non-linear fitting process to match their respective MRIs. Therefore, we used a weighted sum of the distance from the electrode contact to the surface points on the 3D surfaces to place the electrode in the context of the atlas brain. This was performed using a custom program written in Matlab (Mathworks, Natick, MA) to minimize the error between the electrode position in the patient-specific model and its corresponding position in the anatomical atlas.

Once the electrode locations from each patient were determined in the anatomical atlas, a finite element model (FEM) was used to predict the electric field produced as a function of the stimulation parameters. The tissue properties in the anatomical atlas were estimated from a diffusion tensor imaging (DTI) volume which was acquired using single shot echo planar imaging sequence with an isotropic voxel size of 2.2mm and b-value of 700 mm^2/s (Wakana et al., 2004), and was transformed into 3D electrical conductivity tensors on a per-voxel basis (Tuch et al., 2001). These DTI-based tissue conductivities were then coupled to a 3D finite element electric field model of DBS (McIntyre et al., 2004; Butson et al., 2007b). The electric field was calculated using the Poisson equation and a Fourier FEM solver to determine the time- and space-dependent voltage distribution within the brain as a function of the stimulation parameters (Butson and McIntyre, 2005; Butson et al., 2007b). The predicted spread of stimulation was then expressed as the VTA, the basis of which can be found in our previous publications (Butson and McIntyre, 2005; Butson et al., 2006; Butson and McIntyre, 2006; Butson and McIntyre, 2007). Simulations and VTA predictions were performed using BioPSE (SCI Institute, University of Utah).

Clinically Scored VTAs

For each electrode contact location (n=28) and each set of stimulation parameters (n=163) we calculated a VTA, taking into account the impedance of the electrode-tissue interface (Butson et al., 2006) and the stimulation waveform generated during monopolar stimulation (Butson and McIntyre, 2007). All VTAs were overlaid on a 3-dimensional lattice of the PSA which consisted of approximately 100,000 voxels (Figure 3). We performed our analysis on a voxel by voxel basis without any *a priori* assumptions about which anatomical structures might be directly stimulated by DBS. For each set of stimulation parameters, a raw numerical score for bradykinesia, rigidity, and paresthesia was determined from the clinical evaluation (example data shown in Figure 1, bottom row; Figure 2, top row). The raw scores were normalized to the maximum improvement recorded for each outcome measure across all patients. Every voxel within each VTA was assigned the normalized score for each outcome (Figure 2, bottom row) and after all VTAs had been added, the normalized clinical scores for each voxel were averaged. Isosurfaces were then constructed to encompass regions where stimulation-induced activation resulted in clinical improvement (regions

associated with >50% or >75% improvement are shown in the Results). The end product of this approach was a probabilistic atlas of clinical outcome scores on a per-symptom basis, demonstrated with illustrative data in Figure 3.

RESULTS

Clinical Activation Volumes Produced Therapeutic Effects & Side Effects

163 VTAs were generated across all patients and electrode contact locations (Figure 4A, B). These VTAs encompassed the entire subthalamic region and also intersected parts of the anterolateral thalamus and the internal capsule. The range of clinical outcomes associated with these VTAs included both therapeutic improvements in bradykinesia and rigidity, as well as paresthesias. We first sought to identify which regions were associated with any improvement in each outcome regardless of the magnitude of the effect. To do so we generated a PSA for each individual clinical outcome and then examined interactions between therapeutic improvements and side effects. Using data from our six patient cohort we identified stimulation volumes associated with improvements in bradykinesia or rigidity. These spanned much of the sampled territory encompassing most of the STN, the region associated with zona incerta and fields of Forel (ZI/FF), as well as parts of thalamus and the internal capsule (Figure 4C, D). However, portions of these volumes were also associated with paresthesias, and were unlikely to be useful for therapeutic stimulation. Therefore, we subtracted those regions that showed improvement in bradykinesia and/or rigidity but which were also associated with paresthesias (Figure 4C, D).

Stimulation Targets for Bradykinesia and Rigidity

The results shown in Figure 4 suggest that therapeutic effects from DBS can be achieved by direct stimulation of numerous different anatomical territories in the subthalamic region. However, herein lays one potential advantage to the concept of PSAs. We used our example data, albeit from a limited number of patients, to identify distinct locations for the activation volumes associated with the greatest improvements in specific clinical symptoms. We selected voxels in which stimulation resulted in at least a 50% or 75% improvement in each symptom (normalized to the maximum improvement for the symptom measured across all patients) and identified the anatomical location of their overlap (Figure 5). We found that the stimulation target regions for bradykinesia or rigidity differed in their relative size and were anatomically distinct.

At the >50% improvement level, the stimulation target region for rigidity was relative large, encompassing much of the white matter between thalamus and STN, as well as substantial spread into the anteriolateral thalamus (Figure 5A). When criteria for voxel inclusion were elevated to at least 75% improvement, the rigidity target shrank considerably and become focused on an area dorsal to the central STN (Figure 5B, Talairach coordinates of volume centroid: 13, 10, 0). Bradykinesia improvement at the 50% or greater level had a target region that was dorsal to the posterior STN and was much smaller than the corresponding rigidity target region (Figure 5C). At the >75% level the bradykinesia target shrank and the centroid of the volume moved ventrally (Talairach coordinates: 13, 14, −1). Interestingly, at the 75% or greater improvement level neither the bradykinesia or rigidity target volumes overlapped with any part of the atlas defined borders of the STN. Instead the target volumes were focused on the white matter dorsal to the STN. Each of the 75% improvement target volumes reflect data from at least 10 VTAs among three patients, indicating that the results were not idiosyncratic to outcomes from a single patient.

DISCUSSION

The basic goal of this study was to develop methods to combine patient-specific computational models of DBS with quantitative clinical evaluations. We present an example PSA generated with data from six PD patients with electrodes implanted in the subthalamic region. While the small patient population may limit the explicit value of this particular PSA, the general concept was successfully demonstrated. The continual of addition of new patient data into this PSA has potential to increase its utility for STN DBS for PD, as well as provide a foundation for investigation of other brain stimulation targets. Interestingly, the target volumes predicted by our PSA (Figure 5F) match very well with the target volume used in Frankemolle et al. (Frankemolle et al., 2010) to prospectively predict stimulation parameter settings that were in many was superior to settings defined via traditional clinical methods.

We attempted to define therapeutic stimulation targets by identifying regions of overlapping neural activation volumes associated with marked clinical improvement across multiple patients. Our analysis was performed without *a priori* assumptions on the anatomical entity(ies) directly stimulated. Instead we relied on a voxel-based approach to discretize the entire subthalamic region, thereby enabling correlative analysis between the level of clinical improvement and the probability of stimulation induced neural activation in a given voxel. While our results showed how this could be used to characterize improvement level, there are adjunct maps that capture other important information such as variability and statistical power, each of which vary on a per-voxel basis. In contrast to functional imaging methods such as fMRI where an equivalent amount of data can be gathered for each voxel, our analysis depends on different electrode positions and VTA sizes to sample different regions.

The methodology used in this study could be useful in any DBS application where the precise relationships between electrode placement, stimulation parameter settings, and clinical outcomes remain unclear. For example, clinical trials to evaluate DBS for treatment refractory depression are currently evaluating two different anatomical brain regions (anterior limb of the internal capsule (Malone et al., 2009) or subcallosal cingulate gyrus white matter (Lozano et al., 2008), but in either case limited information currently exists on the specific target stimulation volume for maximal therapeutic benefit. Data from those clinical trials could be used to create PSAs in a similar fashion as performed in this study and provide guidance for subsequent studies on DBS for neuropsychiatric disorders. Similarly, PSAs could be used to refine knowledge on common DBS targets such as the STN or globus pallidus. Our early stage results suggest that maximal therapeutic treatment of both bradykinesia and rigidity were associated with stimulation of the same general area (white matter dorsal to the STN). These results coincide well with previous conclusions derived from similar patient-specific neurostimulation models (Maks et al., 2009; Frankemolle et al., 2010). However, the PSA also indicated that these two symptoms may have distinct targets, which if substantiated by future studies with larger sample sizes and data from multiple institutions could have important implications for surgical targeting and device programming.

Possible Physiological Origin of Distinct Stimulation Targets

Numerous prior publications have concluded that the STN per se may not be the only stimulation target with the subthalamic region (Plaha et al., 2006; Maks et al., 2009). The unique contribution of this study was a methodology to quantitatively distinguish between stimulation targets on a per-symptom basis (Figure 5). Given the currently achievable surgical accuracy for DBS electrode placement to within ~2 mm of the desired target (Maciunas et al., 1994; Holloway et al., 2005), our results suggest that it could be possible to tailor electrode placement to the specific target volume associated with a given symptom.

Likewise it should be possible to effectively stimulate multiple targets with an electrode that can activate multiple target regions via advanced techniques such as current steering (Butson and McIntyre, 2008) and/or directionally oriented electrode contacts.

The predominant neural elements within our predicted target regions are axonal in nature, embedded in fiber bundles consisting of efferent axons (e.g. emanating from STN, substantia nigra, ZI), afferent axons (e.g. arriving from pallidum, cortex), and fibers of passage (e.g. lenticular fasciculus, prelemniscal radiation). The electric field induced by DBS (Miocinovic et al., 2009) is non-discriminately applied to all of these neural elements. Both theoretical (Miocinovic et al., 2006) and experimental (Hashimoto et al., 2003) results suggest that the stimulation generates propagating action potentials in these neurons. When neurons are stimulated, the action potential initiates in the axon, even if the neurons' somata is in close proximity to the electrode (Nowak and Bullier, 1998; McIntyre and Grill, 1999). Therefore, our VTA calculations focus on axonal activation and are intended to be representative of the neural response to the broad spectrum of neural elements surrounding the DBS electrode.

While the exact therapeutic mechanisms of DBS remain unclear, a growing body of evidence suggests that stimulation-induced disruption of pathological oscillations throughout the basal-ganglia-thalamocortical circuit plays a major role (Li et al., 2007; Guo et al., 2008; Hahn et al., 2008; Hahn and McIntyre, 2010). Although speculative given our current understanding of the system, three axonal pathways of interest in the target region would be especially well suited to contribute the disruption of pathological oscillations. First are the efferent axons of the STN itself. Second is the lenticular fasciculus (LF), which courses dorsal to the STN and consists of pallidal outflow to the thalamus (Parent and Parent, 2005; Miocinovic et al., 2006). Third is antidromic activation of cortical afferents (Li et al., 2007; Gradinaru et al., 2009).

Cortical afferents and the LF have previously been implicated in the mechanisms of DBS and their relative anatomical arrangement in the subthalamic region provide for interesting connections to the results of this study (Figure 5). Therapeutic benefits from rigidity can often be achieved through different contact locations in the subthalamic region, and much of the cortical inputs to the subthalamic region approach from the antero-dorsal direction over a dispersed area (Nambu et al., 1997), corresponding to a relatively large target volume for rigidity (Figure 5A). Conversely, the LF is a more focused fiber bundle coursing by the postero-medial border of the STN on its way into thalamus (Parent and Parent, 2004), corresponding to a relatively smaller target volume for bradykinesia (Figure 5C). While speculative, these two examples demonstrate how PSAs are a new tool to help identify possible neuroanatomical relationships that connect therapeutic outcomes and DBS technology.

Maximizing Clinical Outcomes

The use of DBS can be compared to the use of medication, in the sense that the neurostimulation "prescription" consists of synergistic interaction between the electrode location and stimulation parameter settings. The electrode location is chosen intra-operatively based on the patient anatomy, imaging data, and intra-operative electrophysiology (Machado et al., 2006). The stimulation parameters are defined post-operatively, titrated to provide maximal therapeutic benefit with minimal side effects (Volkmann et al., 2006). DBS PSAs could be used to assist both of these steps. Specifically, pre-operative targeting could be based not only on the patient anatomy but also on the patient's primary symptoms. For example, the results of this study suggest that rigidity dominant patients might benefit from electrodes implanted more anteriorly than for bradykinesia dominant patients. Further, the target stimulation volumes could be combined

with patient-specific VTA predictions to select stimulation parameters that optimally activate the target region (Butson et al., 2007b; Frankemolle et al., 2010). Such concepts could be integrated into surgical planning and clinical programming software technologies intended to provide cutting edge advances in image registration, brain atlases, and computational modeling to real world clinical applications (Finnis et al., 2003; D'Haese et al., 2005; Nowinski et al., 2005; Butson et al., 2007a; Miocinovic et al., 2007; Yelnik et al., 2007; Bardinet et al., 2009).

Limitations and Sources of Error

While this study provides quantitative information about areas which should be stimulated and others that should be avoided, there are several limitations and possible sources of error in our analysis. With regard to the clinical evaluation, patients were tested with the ipsilateral stimulator turned on, programmed with therapeutic stimulation settings that were arrived at pragmatically based on clinical judgment and experience, independently of this study. While ipsilateral clinical benefit is a possible confound, we expect that such an effect on our results is minimal because the effects of contralateral stimulation would be superimposed on a constant, background reduction in symptoms. The primary outcomes of the patient evaluation were quantitative measures of bradykinesia and rigidity. Detailed analysis of overall clinical outcomes in terms of Hoehn & Yahr staging, UPDRS-III and quality of life measures was not performed, although these outcomes are amenable to analysis using a PSA and could be included in future work.

There are also methodological considerations with regard to the computational modeling. First, the spatial extent of the volumes of activation evaluated in this study was limited by the electrode locations and the size of the corresponding VTAs, which in turn were limited by the range of stimulation amplitudes that each patient could tolerate. However, given the distribution of electrode contacts across the various patients we were able to sample the entire subthalamic region and adequately explore locations associated with therapeutic benefit (Figure 4B). A second possible source of error stems from image coregistration. We attempted to minimize error between pre- and post-operative patient images by using widely accepted coregistration algorithms (ITK 3D registration in Analyze). This approach works well when registering images taken on the same patient by maximizing the similarity over the entire brain. For atlas registration, we used T1 weighted images for both the patient and atlas brains, and employed an approach that maximized accuracy in the immediate vicinity of the electrode relative to the surrounding anatomical nuclei (see Methods). Further, we took great care to confirm the relative placement of the electrode and surrounding nuclei in both the patient and atlas models by visual inspection. Another possible source of error was in our VTA predictions. VTAs were generated from detailed bioelectric field models combined with activation function-based predictions of the neural response to DBS. We have conducted extensive studies in attempts to validate the model predictions (Butson et al., 2007b; Miocinovic et al., 2009; Chaturvedi et al., 2010); however, it should be noted that the neurostimulation models used in this study cannot capture all of the possible neural responses to DBS. Lastly, the small number of patients in this study precludes us from making definitive statements with regard to stimulation targets for STN DBS patients.

Conclusion

This study presents methods to construct a probabilistic atlas of stimulation-induced activation during DBS. These methods were developed during prospective clinical evaluation of patients with DBS in the STN region. However, we propose that this approach could be used to augment the study of DBS in any part of the brain and may prove useful in quantifying any number of motor and/or non-motor outcomes from DBS. DBS PSAs could be especially useful in the study of emerging indications such as epilepsy and

neuropsychiatric disorders, accelerating the identification of optimal surgical targets and stimulation parameter settings.

RESEARCH HIGHLIGHTS

- Probabilistic stimulation atlas for deep brain stimulation
- Patient-specific computational models define volume of tissue activated
- Activation volumes coupled with clinical outcomes measures to define target stimulation regions
- DBS for Parkinson's disease is associated with target volumes dorsal to the subthalamic nucleus

Acknowledgments

This work was supported by grants from the National Institutes of Health (grant numbers: R21 NS050449, F32 NS052042, R01 NS059736). BioPSE software was made possible in part by a grant from the NIH/NCRR Center for Integrative Biomedical Computing, P41-RR12553-10. The authors would like to thank Susumu Mori for providing the diffusion tensor brain atlas and Kevin Wang for assistance with analysis of the clinical data.

References

Baker KB, Tkach JA, Nyenhuis JA, Phillips M, Shellock FG, Gonzalez-Martinez J, Rezai AR. Evaluation of specific absorption rate as a dosimeter of MRI-related implant heating. J Magn Reson Imaging 2004;20:315–320. [PubMed: 15269959]

Bardinet E, Bhattacharjee M, Dormont D, Pidoux B, Malandain G, Schupbach M, Ayache N, Cornu P, Agid Y, Yelnik J. A three-dimensional histological atlas of the human basal ganglia. II. Atlas deformation strategy and evaluation in deep brain stimulation for Parkinson disease. J Neurosurg 2009;110:208–219. [PubMed: 18976051]

Butson CR, McIntyre CC. Tissue and electrode capacitance reduce neural activation volumes during deep brain stimulation. Clin Neurophysiol 2005;116:2490–2500. [PubMed: 16125463]

Butson CR, McIntyre CC. Role of electrode design on the volume of tissue activated during deep brain stimulation. J Neural Eng 2006;3:1–8. [PubMed: 16510937]

Butson CR, McIntyre CC. Differences among implanted pulse generator waveforms cause variations in the neural response to deep brain stimulation. Clin Neurophysiol 2007;118:1889–1894. [PubMed: 17581776]

Butson CR, McIntyre CC. Current steering to control the volume of tissue activated during deep brain stimulation. Brain Stimulation 2008;1:7–15. [PubMed: 19142235]

Butson CR, Maks CB, McIntyre CC. Sources and effects of electrode impedance during deep brain stimulation. Clin Neurophysiol 2006;117:447–454. [PubMed: 16376143]

Butson CR, Noecker AM, Maks CB, McIntyre CC. StimExplorer: Deep brain stimulation parameter selection software system. Acta Neurochir Suppl (Wien) 2007a;97:569–574.

Butson CR, Cooper SE, Henderson JM, McIntyre CC. Patient-specific analysis of the volume of tissue activated during deep brain stimulation. NeuroImage 2007b;34:661–670. [PubMed: 17113789]

Chaturvedi A, Butson CR, Lempka SF, Cooper SE, McIntyre CC. Patient-specific models of deep brain stimulation: Influence of field model complexity on neural activation predictions. Brain Stimulation. 2010 In Press.

Christensen GE, Joshi SC, Miller MI. Volumetric transformation of brain anatomy. IEEE Trans Med Imaging 1997;16:864–877. [PubMed: 9533586]

D'Haese PF, Cetinkaya E, Konrad PE, Kao C, Dawant BM. Computer-aided placement of deep brain stimulators: from planning to intraoperative guidance. IEEE Trans Med Imaging 2005;24:1469–1478. [PubMed: 16279083]

Finnis KW, Starreveld YP, Parrent AG, Sadikot AF, Peters TM. Three-dimensional database of subcortical electrophysiology for image-guided stereotactic functional neurosurgery. IEEE Trans Med Imaging 2003;22:93–104. [PubMed: 12703763]

Frankemolle AM, Wu J, Noecker AM, Voelcker-Rehage C, Ho JC, Vitek JL, McIntyre CC, Alberts JL. Reversing cognitive-motor impairments in Parkinson's disease patients using a computational modelling approach to deep brain stimulation programming. Brain 2010;133:746–761. [PubMed: 20061324]

Gradinaru V, Mogri M, Thompson KR, Henderson JM, Deisseroth K. Optical Deconstruction of Parkinsonian Neural Circuitry. Science. 2009

Guehl D, Vital A, Cuny E, Spampinato U, Rougier A, Bioulac B, Burbaud P. Postmortem proof of effectiveness of zona incerta stimulation in Parkinson disease. Neurology 2008;70:1489–1490. [PubMed: 18413572]

Guo Y, Rubin JE, McIntyre CC, Vitek JL, Terman D. Thalamocortical relay fidelity varies across subthalamic nucleus deep brain stimulation protocols in a data-driven computational model. J Neurophysiol 2008;99:1477–1492. [PubMed: 18171706]

Hahn PJ, McIntyre CC. Modeling shifts in the rate and pattern of subthalamopallidal network activity during deep brain stimulation. J Comput Neurosci. 2010

Hahn PJ, Russo GS, Hashimoto T, Miocinovic S, Xu W, McIntyre CC, Vitek JL. Pallidal burst activity during therapeutic deep brain stimulation. Exp Neurol 2008;211:243–251. [PubMed: 18355810]

Hashimoto T, Elder CM, Okun MS, Patrick SK, Vitek JL. Stimulation of the subthalamic nucleus changes the firing pattern of pallidal neurons. J Neurosci 2003;23:1916–1923. [PubMed: 12629196]

Holloway KL, Gaede SE, Starr PA, Rosenow JM, Ramakrishnan V, Henderson JM. Frameless stereotaxy using bone fiducial markers for deep brain stimulation. J Neurosurg 2005;103:404–413. [PubMed: 16235670]

Lemaire JJ, Coste J, Ouchchane L, Caire F, Nuti C, Derost P, Cristini V, Gabrillargues J, Hemm S, Durif F, Chazal J. Brain mapping in stereotactic surgery: a brief overview from the probabilistic targeting to the patient-based anatomic mapping. Neuroimage 2007;37(Suppl 1):S109–115. [PubMed: 17644002]

Li S, Arbuthnott GW, Jutras MJ, Goldberg JA, Jaeger D. Resonant antidromic cortical circuit activation as a consequence of high-frequency subthalamic deep-brain stimulation. J Neurophysiol 2007;98:3525–3537. [PubMed: 17928554]

Lozano AM, Mayberg HS, Giacobbe P, Hamani C, Craddock RC, Kennedy SH. Subcallosal cingulate gyrus deep brain stimulation for treatment-resistant depression. Biol Psychiatry 2008;64:461–467. [PubMed: 18639234]

Machado A, Rezai AR, Kopell BH, Gross RE, Sharan AD, Benabid AL. Deep brain stimulation for Parkinson's disease: surgical technique and perioperative management. Mov Disord 2006;21(Suppl 14):S247–258. [PubMed: 16810722]

Maciunas RJ, Galloway RL Jr, Latimer JW. The application accuracy of stereotactic frames. Neurosurgery 1994;35:682–694. discussion 694–685. [PubMed: 7808612]

Maks CB, Butson CR, Walter BL, Vitek JL, McIntyre CC. Deep brain stimulation activation volumes and their association with neurophysiological mapping and therapeutic outcomes. J Neurol Neurosurg Psychiatry. 2009 In Press.

Malone DA Jr, Dougherty DD, Rezai AR, Carpenter LL, Friehs GM, Eskandar EN, Rauch SL, Rasmussen SA, Machado AG, Kubu CS, Tyrka AR, Price LH, Stypulkowski PH, Giftakis JE, Rise MT, Malloy PF, Salloway SP, Greenberg BD. Deep brain stimulation of the ventral capsule/ventral striatum for treatment-resistant depression. Biol Psychiatry 2009;65:267–275. [PubMed: 18842257]

McIntyre CC, Grill WM. Excitation of central nervous system neurons by nonuniform electric fields. Biophys J 1999;76:878–888. [PubMed: 9929489]

McIntyre CC, Mori S, Sherman DL, Thakor NV, Vitek JL. Electric field and stimulating influence generated by deep brain stimulation of the subthalamic nucleus. Clin Neurophysiol 2004;115:589–595. [PubMed: 15036055]

Miocinovic S, Maks CB, Noecker AM, Butson CR, McIntyre CC. Cicerone: Deep brain stimulation neurosurgical navigation software system. Acta Neurochir Suppl (Wien) 2007;97:561–567.

Miocinovic S, Parent M, Butson CR, Hahn PJ, Russo GS, Vitek JL, McIntyre CC. Computational analysis of subthalamic nucleus and lenticular fasciculus activation during therapeutic deep brain stimulation. J Neurophysiol 2006;96:1569–1580. [PubMed: 16738214]

Miocinovic S, Lempka SF, Russo GS, Maks CB, Butson CR, Sakaie KE, Vitek JL, McIntyre CC. Experimental and theoretical characterization of the voltage distribution generated by deep brain stimulation. Exp Neurol 2009;216:166–176. [PubMed: 19118551]

Nambu A, Tokuno H, Inase M, Takada M. Corticosubthalamic input zones from forelimb representations of the dorsal and ventral divisions of the premotor cortex in the macaque monkey: comparison with the input zones from the primary motor cortex and the supplementary motor area. Neurosci Lett 1997;239:13–16. [PubMed: 9547160]

Nowak LG, Bullier J. Axons, but not cell bodies, are activated by electrical stimulation in cortical gray matter. I. Evidence from chronaxie measurements. Exp Brain Res 1998;118:477–488. [PubMed: 9504843]

Nowinski WL, Belov D, Pollak P, Benabid AL. Statistical analysis of 168 bilateral subthalamic nucleus implantations by means of the probabilistic functional atlas. Neurosurgery 2005;57:319–330. [PubMed: 16234681]

Obeso JA, Olanow CW, Rodriguez-Oroz MC, Krack P, Kumar R, Lang AE. Deep-brain stimulation of the subthalamic nucleus or the pars interna of the globus pallidus in Parkinson's disease. N Engl J Med 2001;345:956–963. [PubMed: 11575287]

Parent M, Parent A. The pallidofugal motor fiber system in primates. Parkinsonism Relat Disord 2004;10:203–211. [PubMed: 15120094]

Parent M, Parent A. Single-axon tracing and three-dimensional reconstruction of centre median-parafascicular thalamic neurons in primates. J Comp Neurol 2005;481:127–144. [PubMed: 15558721]

Patrick SK, Denington AA, Gauthier MJ, Gillard DM, Prochazka A. Quantification of the UPDRS Rigidity Scale. IEEE Trans Neural Syst Rehabil Eng 2001;9:31–41. [PubMed: 11482361]

Plaha P, Ben-Shlomo Y, Patel NK, Gill SS. Stimulation of the caudal zona incerta is superior to stimulation of the subthalamic nucleus in improving contralateral parkinsonism. Brain 2006;129:1732–1747. [PubMed: 16720681]

Schwalb JM, Hamani C. The history and future of deep brain stimulation. Neurotherapeutics 2008;5:3–13. [PubMed: 18164479]

Tuch DS, Wedeen VJ, Dale AM, George JS, Belliveau JW. Conductivity tensor mapping of the human brain using diffusion tensor MRI. Proc Natl Acad Sci U S A 2001;98:11697–11701. [PubMed: 11573005]

Viola P, Wells WMI. Alignment by maximization of mutual information. IJCV 1997;24:137–154.

Volkmann J, Moro E, Pahwa R. Basic algorithms for the programming of deep brain stimulation in Parkinson's disease. Mov Disord 2006;21:S284–S289. [PubMed: 16810675]

Wakana S, Jiang H, Nagae-Poetscher LM, van Zijl PC, Mori S. Fiber tract-based atlas of human white matter anatomy. Radiology 2004;230:77–87. [PubMed: 14645885]

Weaver FM, et al. Bilateral deep brain stimulation vs best medical therapy for patients with advanced Parkinson disease: a randomized controlled trial. JAMA 2009;301:63–73. [PubMed: 19126811]

Yelnik J, Bardinet E, Dormont D, Malandain G, Ourselin S, Tande D, Karachi C, Ayache N, Cornu P, Agid Y. A three-dimensional, histological and deformable atlas of the human basal ganglia. I. Atlas construction based on immunohistochemical and MRI data. Neuroimage 2007;34:618–638. [PubMed: 17110133]

Yelnik J, Damier P, Demeret S, Gervais D, Bardinet E, Bejjani BP, Francois C, Houeto JL, Arnule I, Dormont D, Galanaud D, Pidoux B, Cornu P, Agid Y. Localization of stimulating electrodes in patients with Parkinson disease by using a three-dimensional atlas-magnetic resonance imaging coregistration method. J Neurosurg 2003;99:89–99. [PubMed: 12854749]

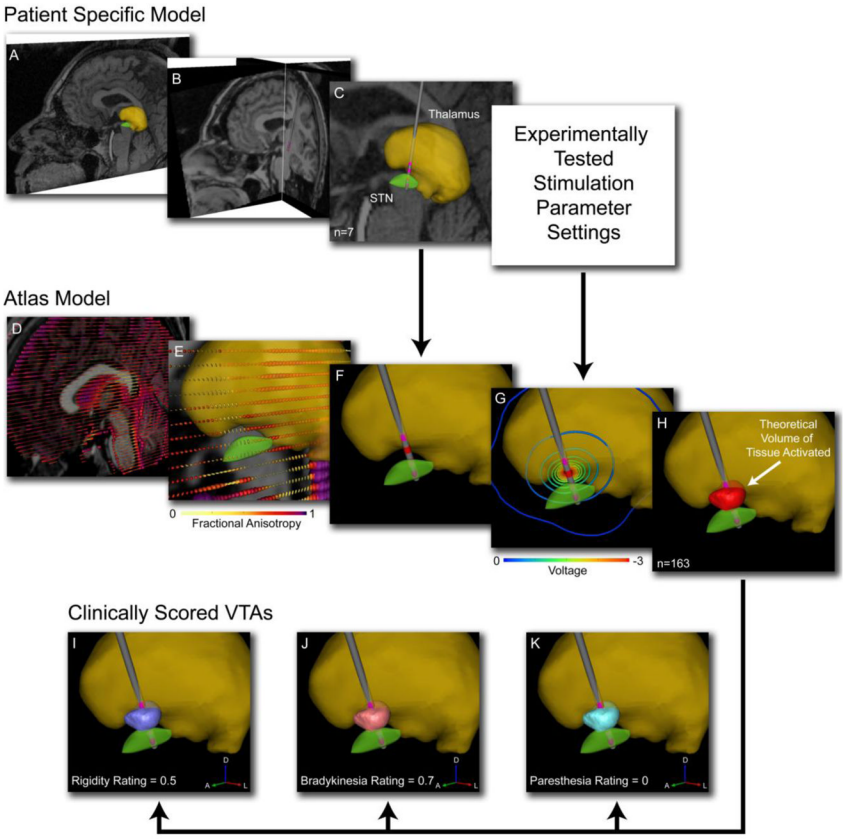

Figure 1.

Patient-specific DBS models. A) 3D nuclei (e.g. thalamus – yellow volume; STN – green volume) were fit to the pre-operative MRI of each subject. B) The pre-operative MRI was co-registered with a post-operative MRI to identify the implanted DBS electrode location (note electrode in coronal slice). C) For each tested hemisphere (n=7) the electrode location was defined relative to the pertinent nuclei. D) Each patient-specific model was transformed into the context of a single atlas brain. The atlas brain included both anatomical and diffusion tensor imaging data and was used to predict neural activation from the stimulation protocol. E) DTI-based conductivity tensors with color indicating fractional anisotropy described the tissue electrical properties. F) Each patient-specific model had a unique DBS electrode location. G) Each experimentally tested stimulation parameter setting resulted in a unique voltage distribution. H) The theoretical volume of tissue activated (VTA) by each tested setting (n=163) was calculated. Each VTA was assigned a clinical score for rigidity (I), bradykinesia (J), and paresthesia (K).

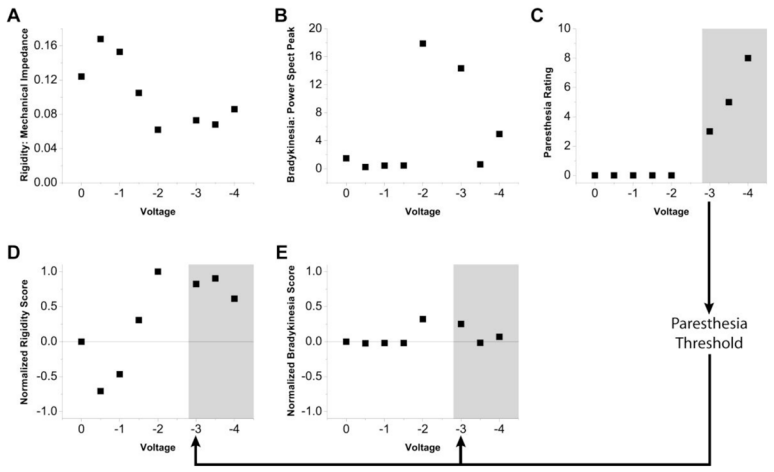

Figure 2.

Clinical Evaluation. Example data from stimulation testing at one electrode contact in one patient. All DBS data were acquired with a fixed stimulation frequency of 130 Hz and a fixed stimulus pulse width of 0.06 ms. A) Rigidity measurements were acquired with a clinical impedance measurement device (model RA-1, NeuroKinetics). Higher values represent greater rigidity. B) Finger tapping bradykinesia measurements were acquired with solid state gyroscopes (model G-1, NeuroKinetics). Higher values represent lower bradykinesia. C) Paresthesias were rated on a 10 point scale as reported by the patient. D) Rigidity and E) Bradykinesia data were rescored on a normalized scale from 1 to −1. Scores above 0 indicate improvement and scores below 0 indicate worsening relative to the OFF DBS baseline. Shaded areas indicate scores above the paresthesia threshold.

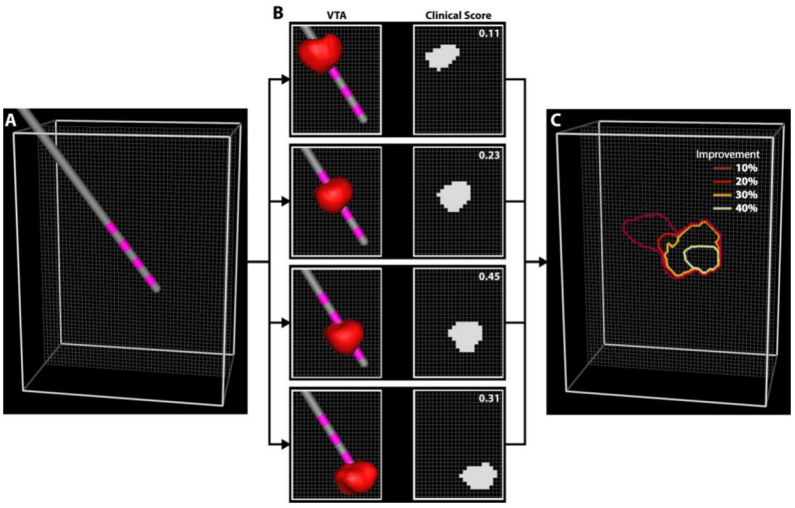

Figure 3.

Probabilistic atlas generation. A) A 3D lattice was constructed to encompass all of the VTAs corresponding to the experimentally tested stimulation parameters. Lattice dimensions were 36 by 52 by 66 voxels where each voxel size is 0.5 mm^3. For clarity, only one cross-sectional slice of the lattice is shown. B) An example VTA is shown for each contact with stimulation settings −4 V, 60 μsec, 130 Hz. Voxels within the VTA were assigned the corresponding normalized clinical score as indicated. C) The probabilistic atlas was created from the average clinical score for each voxel. Regions where stimulation caused therapeutic improvement were delineated by isosurfacing the data to the desired improvement level.

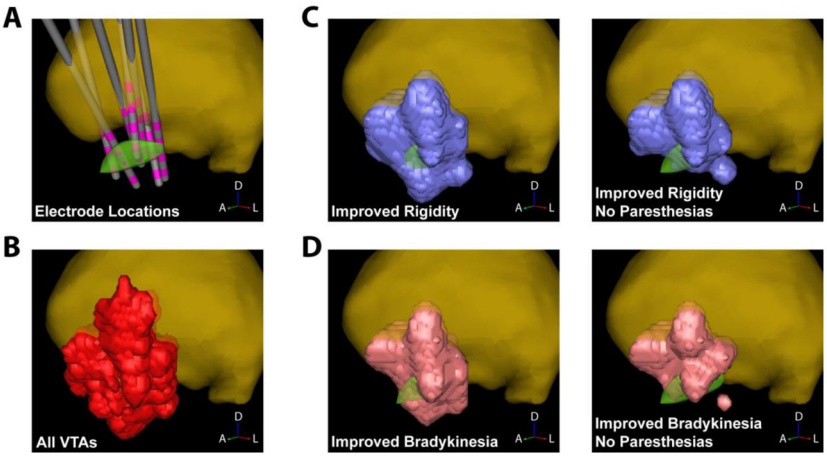

Figure 4.

Clinical outcomes. A) DBS electrode locations for all patients (n=7 hemispheres) in the context of the anatomical atlas. B) VTAs (red volume) generated for all electrode locations and stimulation protocols (n=163 VTAs), shown superimposed on each other. Each VTA had an assigned clinical score for rigidity, bradykinesia, and parathesia. C) Activation volume (blue) associated with any (i.e. greater than zero) improvement in rigidity. D) Activation volume (pink) associated with any improvement in bradykinesia. The left column shows all VTAs that generated some level of therapeutic benefit, while the right column shows only VTAs corresponding to therapeutic stimulation settings that did not produce paresthesias.

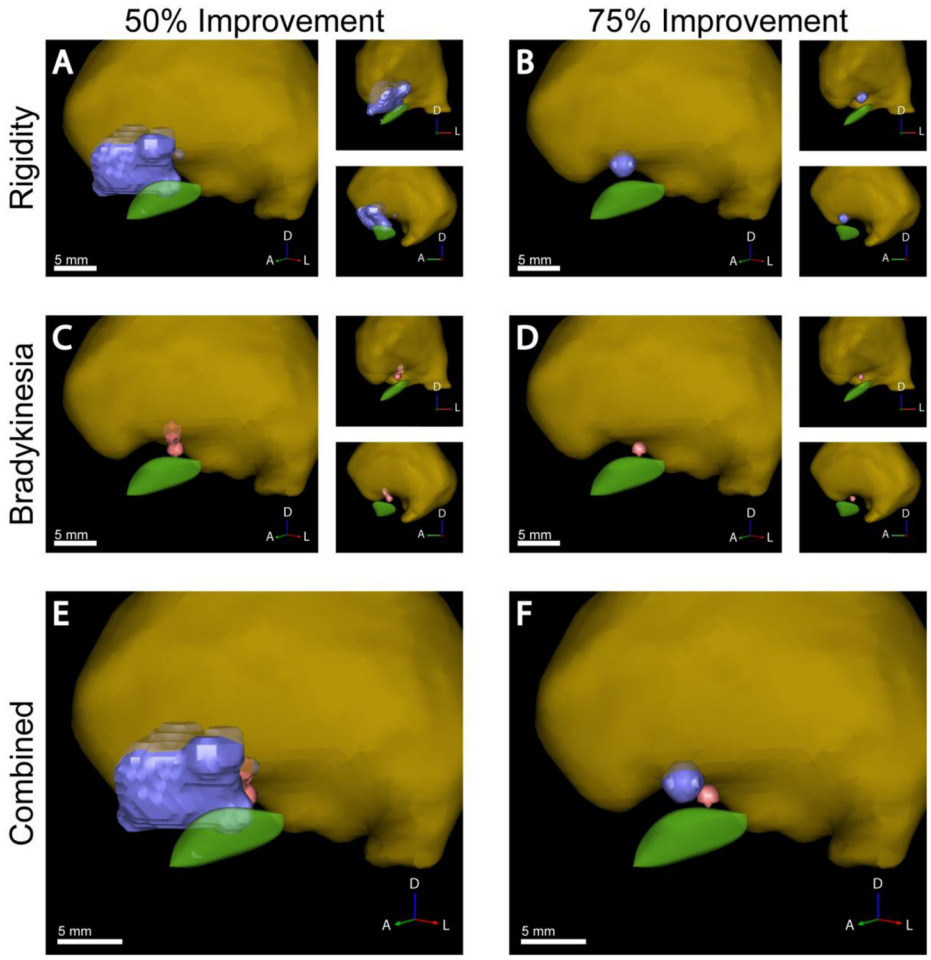

Figure 5.

Probabilistic stimulation targets. Each VTA was voxelized onto a 3D grid of 0.5 mm cubes that encompassed the entire brain region evaluated with DBS. A statistically defined level of clinical improvement was then defined for each voxel based on the VTAs that overlapped with that voxel. The blue volumes indicate the stimulation region associated with at least 50% (A) or 75% (B) improvement in normalized clinical scores of rigidity. The pink volumes indicate at least 50% (C) or 75% (D) improvement in bradykinesia. E,F) Combined rigidity and bradykinesia volumes.

Table 1

Patient Summary. Shown are patient number, primary symptoms, age at experiment, years post-surgery, hemisphere tested, contact number and total number of VTAs. Data shown in the Contact columns indicate electrode impedance as reported by the IPG programmer (Imp) and voltage range tested at that contact (V).

						Contact				
Patient	**Primary Symptoms**	**Age at exp**	**Years post-surg.**	**Hemisphere**		**0**	**1**	**2**	**3**	**Number of VTAs**
1	Bradykinesia, Rigidity	49	1.9	Left	***Imp***	High	High	High	High	
					V	0 to −4	0 to −4.5	0 to −4	0 to −4.5	33
				Right	***Imp***	High	High	High	High	
					V	0 to −2	0 to −2	0 to −2.5	0 to −2.5	18
2	Gait, Freezing, Bradykinesia	61	2.5	Right	***Imp***	High	High	High	Med	
					V	0 to −2	0 to −3	0 to −4	0 to −4	13
3	Tremor, Freezing, Balance	63	4.1	Left	***Imp***	High	High	High	High	
					V	0 to −1	0 to −3	0 to −4	0 to −4	12
4	Rigidity, Bradykinesia	65	2.1	Left	***Imp***	Med	Med	Med	Med	
					V	0 to −5	0 to −5	0 to −6	0 to −5	21
5	Rigidity, Bradykinesia, Tremor	59	0.5	Left	***Imp***	High	High	High	High	
					V	0 to −4	0 to −5	0 to −7	0 to −9	25
6	Freezing, Dyskinesias, Tremor	72	1.1	Left	***Imp***	High	High	High	High	
					V	0 to −4.5	0 to −5	0 to −10	0 to −10	41
	Average (years)	61.5	2.0						**Total**	163